Spectrochimica Acta Part A: Molecular and Biomolecular Spectroscopy 187 (2017) 15–22

Contents lists available at ScienceDirect

Spectrochimica Acta Part A: Molecular and Biomolecular Spectroscopy

journal homepage: www.elsevier.com/locate/saa

Raman spectroscopy differentiates between sensitive and resistant multiple myeloma cell lines

Domenico Franco [a], Sebastiano Trusso [b,*], Enza Fazio [c], Alessandro Allegra [d], Caterina Musolino [d], Antonio Speciale [a], Francesco Cimino [a], Antonella Saija [a], Fortunato Neri [c], Marco S. Nicolò [a], Salvatore P.P. Guglielmino [a,*]

[a] Department of Chemical, Biological, Pharmaceutical and Environmental Sciences, University of Messina, Italy
[b] Institute of Chemical-Physical Processes (IPCF)-CNR, Messina, Italy
[c] Department of Mathematical and Computational Sciences, Physical Science and Earth Science, University of Messina, Italy
[d] Division of Hematology, Department of General Surgery, Pathological Anatomy and Oncology, University of Messina, Italy

ARTICLE INFO

Article history:
Received 7 March 2017
Received in revised form 22 May 2017
Accepted 15 June 2017
Available online 15 June 2017

Keywords:
Multiple myeloma cell line
Drug resistance
Rapid identification
Raman spectroscopy
PCA analysis

ABSTRACT

Current methods for identifying neoplastic cells and discerning them from their normal counterparts are often nonspecific and biologically perturbing. Here, we show that single-cell micro-Raman spectroscopy can be used to discriminate between resistant and sensitive multiple myeloma cell lines based on their highly reproducible biomolecular spectral signatures. In order to demonstrate robustness of the proposed approach, we used two different cell lines of multiple myeloma, namely MM.1S and U266B1, and their counterparts MM.1R and U266/BTZ-R subtypes, resistant to dexamethasone and bortezomib, respectively. Then, micro-Raman spectroscopy provides an easily accurate and noninvasive method for cancer detection for both research and clinical environments. Characteristic peaks, mostly due to different DNA/RNA ratio, nucleic acids, lipids and protein concentrations, allow for discerning the sensitive and resistant subtypes. We also explored principal component analysis (PCA) for resistant cell identification and classification. Sensitive and resistant cells form distinct clusters that can be defined using just two principal components. The identification of drug-resistant cells by confocal micro-Raman spectroscopy is thus proposed as a clinical tool to assess the development of resistance to glucocorticoids and proteasome inhibitors in myeloma cells.

1. Introduction

Multiple myeloma (MM) is a clonal accumulative disease of mature plasma cells which is generally fatal. Despite some drugs are considered as promising therapies for MM [1], resistance still arises in MM subjects [2,3]. In fact, the acquisition of anti-cancer drug resistance is a major issue with treatments in MM [4], since some subjects failed to respond to therapy, due to primary refractoriness and acquisition of resistance [5]. Bortezomib (BTZ) is a first-in-class proteasome inhibitor developed specifically for use as antineoplastic agent [6]. It is a boronic acid dipeptide that is highly selective for inhibition of the chymotryptic activity of the 26S proteasome via reversible binding of its target, PSMB5, a subunit of the 20s catalytic core. BTZ treatment has been shown to inhibit the transcriptional activity of NF-κB as well as trigger the unfolded protein response (UPR), leading to cell stress and apoptosis [7]. It is the most potent antineoplastic agent for the treatment of MM, and a total of 73% of patients with myeloma responded to treatment with BTZ combined with pegylated liposomal doxorubicin [2]. On the other hand, dexamethasone (DXM), a synthetic glucocorticoid steroid hormone, has been generally utilized in the treatment of MM. DXM operates via numerous possible mechanisms. DXM may provoke cell cycle arrest at the G1 phase and the cell cycle arrest may operate as an apoptotic signal [8,9]. Moreover, DXM causes apoptosis through transcription activation of apoptotic genes for Caspase-3, Caspase-8 and Bim proteins [10–13] and suppression of the Akt-PI3K pathway or glucocorticoid receptor (GR) involvement [14–17]. A main problem in treatment of MM is the emergence of cells resistance to drug-induced apoptosis. In fact, because MM is characterized by a complex genomic instability and cytogenetic constitution, chronic exposure to drug may lead to resistant subtypes in subjects with MM, making unnecessary the continuation of therapy. Numerous mechanisms have been found that account for the resistance to BTZ and DXM induced apoptosis, including drug receptor mutations, insufficient ligand, abnormal drug translocation, overexpression of Bcl-2, up-regulation of anti-oxidant proteins, and overexpression of anti-apoptotic proteins [18–22]. Liu et al. [23] demonstrated that interleukin-6 and JAK2/STAT3 signaling mediate the DXM resistance in MM cells,

* Corresponding authors.
E-mail addresses: trusso@me.cnr.it (S. Trusso), sguglielm@unime.it (S.P.P. Guglielmino).

http://dx.doi.org/10.1016/j.saa.2017.06.020
1386-1425/

while other studies have uncovered a role for miR-221-222 in MM DXM resistance [24]. Differently, the mutation in the proteasome β5 subunit (PSMB5), and the increased expression of proteasome, have been shown in cancer cells with acquired resistance to BTZ [25], while activation of NF-κB with inactivating abnormality of TNF receptor-associated factor 3 (TRAF3), in MM cells harboring genetic mutation of NF-κB pathways, has been correlated with BTZ sensitivity [26]. To identify chemoresistance, the characteristics of cancer cells having resistant phenotype to anti-cancer drugs need to be understood, and few complex methods have been proposed to recognize these cancer cells, such as a proteomic identification and clonogenic assays [27,28]. For example, differences in nuclear textures of myeloma cell sub-lines resistant to glucocorticoids (GCs) were observed by image cytometry and the degree of resistance was related to a progressive chromatin condensation [29]. Other studies have evaluated the role of mitochondrial genes including CYPD, SOD2 and MCU on BTZ resistance. These genes were differentially expressed in BTZ-resistant KMS cells. Thus, changes in the expression of these genes lead to changes in mitochondrial activity and in BTZ susceptibility or resistance, and their combined effect contributes to differential sensitivity or resistance of MM cells to BTZ. In support of this finding, coadministration of BTZ and 2-methoxyestradiol, a SOD inhibitor, rendered KMS20 cells sensitive to apoptosis [30].

Hence, induction of resistance to drug in the multiple myeloma is not often associated with significant variations in the cell phenotype, so the identification of resistant cells remains uneasy.

Therefore, in order to address the appropriate pharmacological choice, also ensuring therapeutic success, a fast method for identification chemoresistant cells is need. In this contest, some researchers used specific spectral information, obtained by micro-Raman measurements, to define molecular changes induced by chemotherapeutic [31].

Raman spectroscopy, due to its fingerprint character, can be used to detect the structural changes that take place in cancer cells. Raman scattering in fact involves the interaction of a probe with the vibrational energetic levels within a molecule. Vibrations of specific functional groups lead to the appearance of spectral bands whose intensities and positions provide information regarding the sample's structural properties and can optically probe the molecular changes associated with diseased tissues [32,33]. Moreover, Raman scattering can be used for deriving direct chemical/structural information in a label-free, nondestructive, and real-time manner at the single-cell level, without requiring any exogenous modification of samples [34].

In this work, we analyze by micro-Raman spectroscopy two ~~model~~ cell lines of myeloma multiple, namely MM.1 and U266.B1, before and after resistant acquisition to DXM and BTZ, respectively. Specifically, we compare local and global molecular information, obtained by Raman spectroscopy on several cells within the same cell line, to detect and understand the intracellular biochemical changes that occur in chemoresistant cells.

Furthermore, we evaluate the capability of the micro-Raman spectroscopic technique at single-cell level to discriminate between sensitive and -resistant cells.

MM1.S and MM1.R cells are closely related cell lines and established as a good model to explore mechanisms of resistance to DXM, showing morphology typical of myeloma cell [35]. We outline that one of these cells has a congenital resistance as lacking the receptor for DXM, the other cell acquires it with exposure to BTZ. Since the establishment of the original MM.1 cells, the two cell lines subtypes were developed: 1) a GC-sensitive cell line, namely MM.1S, is identified by the ability of DXM to inhibit cell proliferation and induce apoptosis; 2) the resistant variant, designated MM.1R, was isolated from the original culture based on their lack of responsiveness to DXM-induced cytolysis, due to the non-expression of GR. The cell lines subtypes differ only in their sensitivity to GCs. U266B1 cell line has been used to explore mechanisms of resistance to BTZ. Differently from MM.1R, resistance to BTZ is established exposing U266B1 cultures to gradually increasing concentrations of drug. It is known that U266 BTZ-resistant cells show a relatively less inhibitory effect of prosurvival NF-κB signaling by BTZ and a different regulation of genes related to ubiquitination [36]. Then, principal component analysis (PCA) and subsequent hierarchical component analysis (HCA) were used as fast and reproducible analysis method to discriminate drug-resistant and -sensitive cells.

2. Materials and Methods

2.1. Cell Lines and Culture Conditions

MM.1S, MM.1R and U266B1 were purchased from the American Type Culture Collection (ATCC; Rockville, MD, USA). MM.1S (ATCC® CRL-2974™), MM.1R (ATCC® CRL-2975™) and U266B1(ATCC® TIB-196™) cell lines were cultured in RPMI 1640 medium supplemented with 10% fetal bovine serum (FBS), 100 units/mL penicillin, 100 μg/mL streptomycin, and 2 mM L-glutamine (Sigma-Aldrich, Milan, Italy). Cells were maintained in an incubator with humidified atmosphere containing 5% CO_2 at 37 °C. MM.1S and MM.1R are mixed cell cultures growing both as a lightly attached monolayer and in suspension. Subcultures were prepared by scraping the adherent cells into the medium containing the floating cells, collecting the cells by centrifugation, resuspending the cell pellet in fresh medium and dispensing it into new flasks.

U266B1 is a suspension cell culture; subcultures were prepared collecting cells by centrifugation, resuspending the cell pellet in fresh medium and dispensing into new flasks.

A BTZ-resistant cell line (U266/BTZ-R) was established from its parental line U266B1 according to the protocol developed by Schoester et al. [37]. Briefly, U266B1 were cultured weekly with gradually increasing concentrations of BTZ (Santa Cruz Biotechnology Inc.; Dallas, TX, USA) for 4 h.

During establishment of the U266/BTZ-R cell line, every 48–72 h an aliquot of cells was harvested in order to evaluate cell viability by trypan blue assay. In BTZ-treatment days cell aliquots were harvested at the end of the 4 h exposure to the drug. The percentage of cell viability was calculated by dividing the number of viable cells by the total number of cells and multiplying by 100. The percentage of cell viability, shown as mean ± SD of three determinations, was calculated by dividing the number of viable cells by the total number of cells and multiplying by 100.

BTZ concentration was increased from 1 nM to 32 nM, with stepwise increments of 3.5 nM, in a period of 10 weeks and then followed by weekly exposures to 16 nM of BTZ for 4 h in order to maintain cell resistance. A control U266B1 cell line, not exposed to BTZ, was cultured in parallel with the same subculturing procedure. Before each subculturing passage low-speed centrifugation (100 ×*g* for 5 min) of cell suspension was performed to minimize cell debris and dead cells.

For all the experiments, BTZ was always freshly dissolved in RPMI 1640 medium and immediately used.

To confirm resistance to BTZ, cell viability was evaluated by trypan blue assay performed 48 h after 4 h of exposure to BTZ (10 nM to 10 μM). U266/BTZ-R cell line (BTZ $IC_{50} > 5$ μM) was around 35-fold more resistant to BTZ than control cells (IC_{50} = 146 nM CL 95% 134–163 nM) and retained parental doubling time and morphology.

2.2. Sample Preparation

In order to measure the average number of viable cells, before carrying out Raman spectroscopic analysis, samples from each cell culture were stained with Trypan Blue (Sigma-Aldrich, Milan, Italy) and counted. Low-speed centrifugation (100 ×*g* for 5 min) of cell suspension was performed to minimize eventual presence of cell debris and dead cells. Then, supernatant was removed, cells were resuspended in Phosphate Buffer Saline (PBS, Sigma-Aldrich, Milan, Italy), and 1×10^6 viable cells/mL were centrifuged at 500 ×*g* for

5 min and washed twice in PBS to remove all traces of culture medium. Finally, 50 μL of cell suspension were deposed on a CaF_2 slide treated with 0.01% polylysine (Sigma-Aldrich, Milan, Italy). Each sample was fixed by air-drying in sterile conditions for 15 min. All tests were performed in triplicate. For each cell line, cell viability was always above 95%. Cells with an alterated optical cell morphology have been excluded from Raman measurements.

2.3. Raman Spectroscopy

The spectral differences between MM.1S and MM.1R cells were investigated by means of micro-Raman spectroscopy. A diode laser operating at 2.33 eV (532 nm) was used as an excitation source. Raman spectra were recorded in air at room temperature (RT) using an Olympus BX40 microscope coupled to a Horiba monochromator, equipped with a 600 line/mm holographic grating and to a Peltier-cooled charged-coupled device (CCD) sensor (XploRA apparatus). An edge filter blocks Rayleigh scattered light and stray laser lines. Light was focused onto the sample to a spot of 1 μm in diameter using 100× dry microscope objective (Olympus MPlan N) with a numerical aperture (NA) of 0.90. Care was taken to prevent local heating and damage of the samples. In order to minimize laser-induced heating of the specimens a low power irradiation at the sample surface was used (<0.5 mW). The 450–2000 cm^{-1} spectral range was investigated. Wavenumber calibration was done with an accuracy of ± 2 cm^{-1} using the 520.5 cm^{-1} Raman TO phonon line of a crystalline silicon substrate as reference. An acquisition time of 30 s granted a sufficient signal-to-noise (S/N) ratio.

2.4. Variance Analysis

A continuous baseline correction was performed on each Raman spectrum using the adaptive iteratively re-weighted penalized least square algorithm (airPLS) [38], thereafter spectra were smoothed [39] and normalized to their area in order to minimize fluctuations due to signal intensity variations. Finally, variance values are obtained with respect to the mean spectrum.

Preliminarily, in order to evaluate intracellular variability, Raman scattering measurements were performed, repositioning laser spots onto five different locations within the cell. Then, spectra collected by several cells of sample and representative of the response from each cell line subtypes, were used to identify the most significant bands.

2.5. PCA and Second Derivative Analysis

PCA barcode analysis was used to identify Raman spectra belonging to similar cells stages. PCA analysis (in the physical sciences also referred to as Eigenvector analysis) was performed on spectra after the baseline correction, smoothing and area normalization procedures, as reported in previous section. PCA calculations were performed on a slightly different version of the second derivate based barcode analysis [40]. Barcodes were generated as a function of the sign of the second derivative, a threshold value was used to better identify the barcode limits. The threshold value was determined in such a way to avoid the inclusion of extra peaks, due to noise fluctuation around the zero value, and, at the same time, not to exclude significant Raman peaks. The generated barcodes hold information about peaks position and widths while intensity information is lost, being the barcodes height set to 1. To take into consideration also the relative peak intensities we performed a logical AND operation between the barcode and the averaged spectra. In such way, each barcode holds information about position, width and intensity of the marked peak. For smoothing and second derivative calculations, the Savitzky-Golay smoothing-derivative procedure was used [39]. The resulting barcodes were loaded into rows of a matrix, which was used as input for PCA and HCA procedure. The result of a PCA analysis performed on a given data set is a vector which contains the relevance of principal components classified as a function of their variance. Usually, most of the variance is contained in the first three principal components PC 1, PC 2 and PC 3. Thereafter, HCA algorithm is applied to the PCA results in order to separate the data into statistically similar groups. Cosine and correlation coefficient are two methods for evaluating the similarity between spectroscopic features. Similarity between principal components of different Raman spectra is evaluated according to angle cosine formula and correlation coefficient formula [41]. The more near to 1.0 the value of $cos\theta$ or R is, the more similar are the two vectors. Statistical analysis was performed using custom scripts written in Matlab©.

3. Results

3.1. BTZ Resistance Induction in U266B1 Cell Line

BTZ resistance induction in U266B1 cell line were induced by increasing of drug from 1 nM to 32 nM, with stepwise increments of 3.5 nM, in a period of 10 weeks and then followed by weekly exposures to 16 nM of BTZ for 4 h in order to maintain cell resistance.

Fig. 1 shows that only resistant cells survived and, after this dose, viability increased again even after each other increasing treatment (up to 32 nM), finally reaching around 95% at the end of the procedure.

Starting from treatment with 11.5 nM BTZ, cell viability decreased after each treatment reaching a minimum after exposure to 18.5 nM BTZ.

After which cells were weekly exposed to 16 nM of BTZ for 4 h in order to maintain cell resistance. A control U266B1 cell line, not exposed to BTZ, was cultured in parallel with the same subculturing procedure.

Therefore U266B1, U266/BTZ-R, MM.1S and MM.1R cell lines were subjected to Raman spectroscopy analysis.

3.2. Raman Spectroscopy Analysis

Intracellular variability for each cell line was evaluated, repositioning laser spots onto five different locations within the same cell. Details on how the Raman spectra have been collected by each cell are shown in Fig. 2.

Spectra acquired in different cell location does not show a large intracellular variability within a single cell, according to Chan et al. and our previous work for another cell lines [42,43]. These authors attribute low spatial variations to a large nuclear/cell ratio. In fact, in lymphocyte cells, nucleus occupies 80% of cell volume and consequently nuclear features are constantly highlighted by Raman laser. This result indicates that, in these cell types, the random collecting of Raman spectra in arbitrary cell location preserve data reproducibility of tested samples.

A total of 71 spectra were collected to identify the most important spectral differences, between sensitive and resistant cells. All spectra were previously subjected to some data treatment. Firstly, continuous baseline correction was carried out; then, corrected spectra were normalized to their own area and slightly smoothed, as described in the Materials and Methods section.

Representative Raman spectra of MM.1 and U266B1 sensitive and resistant subtypes, with respective standard deviation values, are shown in Fig. 2. No large variations cell-to-cell was observed in U266/BTZ-R, while some difference was present within MM1.R cell line. However relative standard deviation did not exceed the 15% value in correspondence of the most relevant peaks, doing not make cell-to-cell variability significant for the following analysis.

Spectral variations in 450–2000 cm^{-1} region are used to discriminate cell subtypes. To this purpose, Raman features for nucleic acids, proteins, lipids and carbohydrates were identified (see Fig. 3), and their tentative assignment is shown in Table 1.

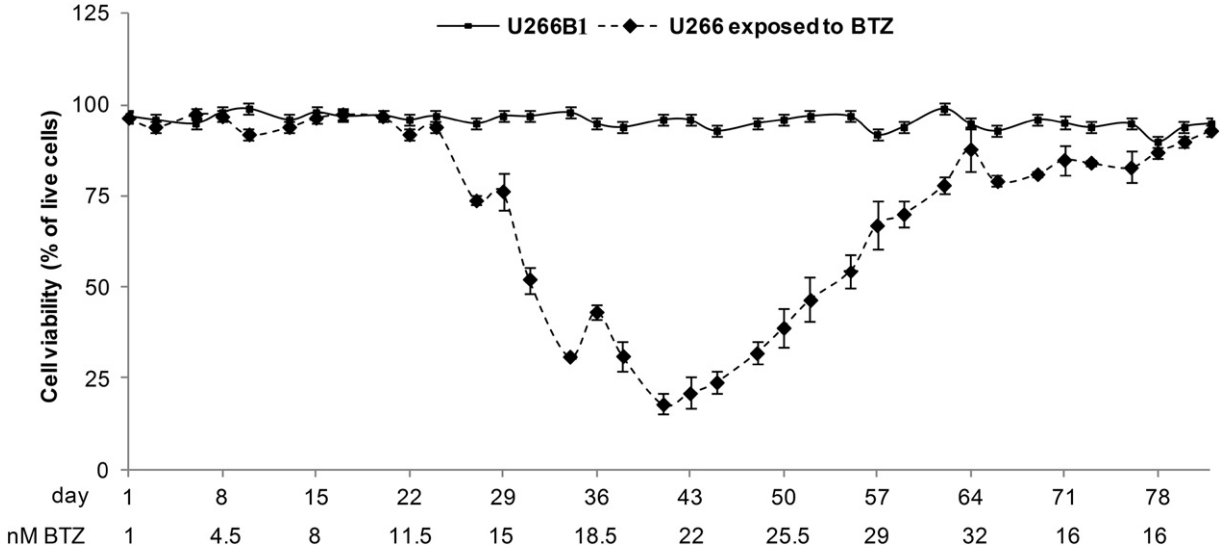

Fig. 1. Cell viability during establishment of the U266 BTZ-resistant cell line (U266/BTZ-R). Then cells were weekly exposed to 16 nM of BTZ for 4 h in order to maintain cell resistance. The percentage of cell viability, shown as mean ± SD of three determinations, was calculated by dividing the number of viable cells by the total number of cells and multiplying by 100.

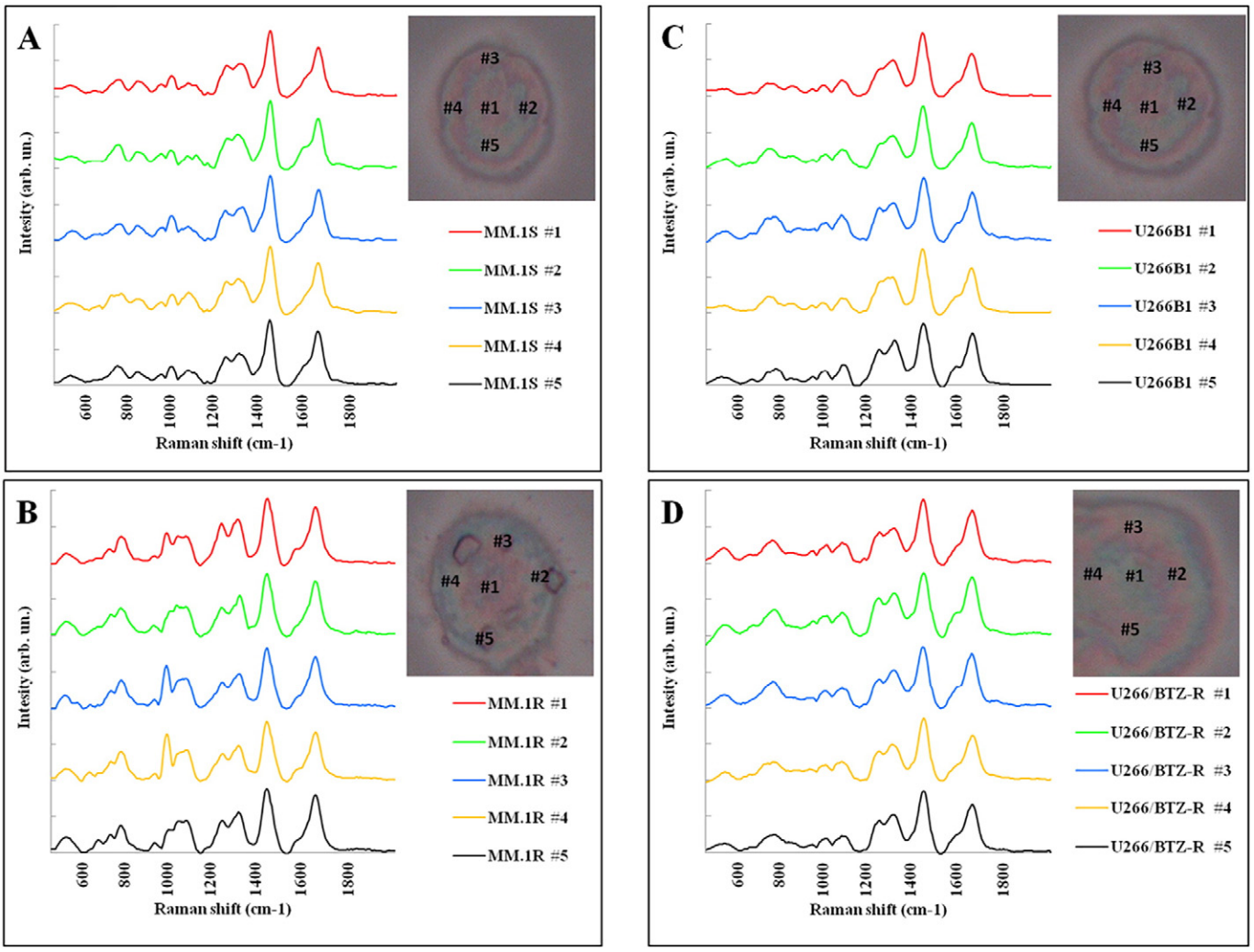

Fig. 2. Raman scattering measurements for each cell of MM.1S (A), MM.1R (B), U266B1 (C) and U266/BTZ-R (D), performed repositioning laser spots onto five different regions within the cell.

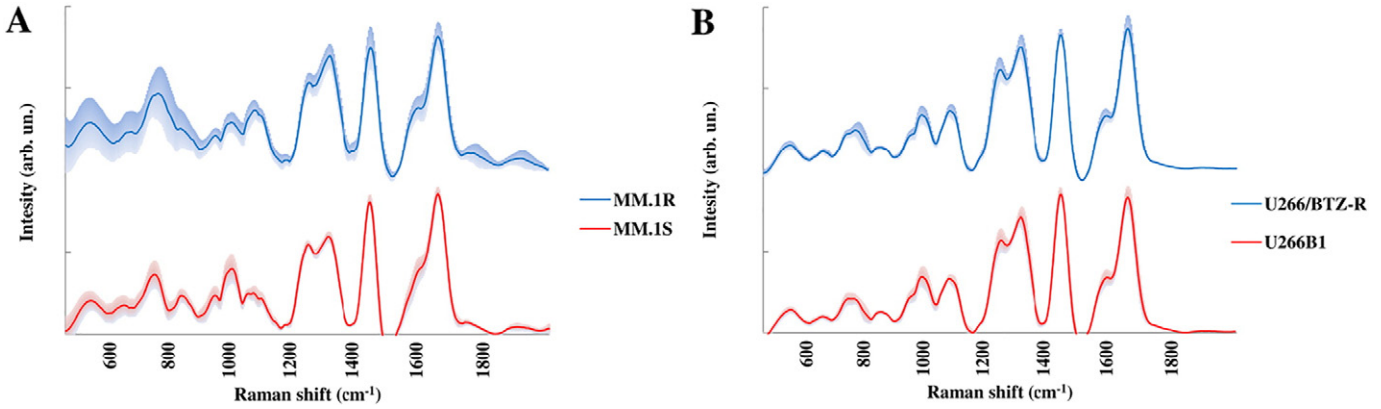

Fig. 3. Mean Raman spectrum (averaged over all the Raman spectra acquired), for MM.1S and MM.1R (A) and for U266B1 and U266/BTZ-R (B) cells. The relative standard deviation values are indicated by the shaded area.

3.3. Raman Features for Discrimination of Sensitive and Resistant Cell Subtypes

The main nucleic acids features in MM.1 and U266B1 cells are exhibited in spectral regions around 650–765 and 1250–1350 cm^{-1}. In these regions the ring breathing modes, ascribable to nucleotide bases, are overlap to protein contributions by amino acids (cysteine, tryptophan and tyrosine) and by secondary protein structures (e.g. α-helix, β-sheets, random coils) of Amide III. The other protein features are exhibited in spectral regions around 995–1015 (ring stretching modes of benzene derivatives) and 1600–1670 (secondary protein structures of Amide I) cm^{-1}. About carbohydrates, main spectral features, ascribable to mono- and disaccharides, are exhibited in the region around 840–860 cm^{-1}. Finally lipid contributions are exhibited in the regions 530–550 (ester group in cholesterol), 960–970 (δ(═CH) wagging) and 1455–1465 (δ(CH_2) wagging) cm^{-1}. Moreover, in the region 1075–1095 contributions of ν(C—C) and ν(C—O) in lipids and O—P—O backbone stretching in nucleic acids and phospholipids are included.

Table 1
Raman band, corresponding to vibrational modes and their assignments [44–50].

Raman band (cm^{-1})	Vibrational mode	Assignment
530–550	Ester group	Cholesterol
650–665	C—S stretching mode	Protein (cysteine)
	C—C twisting aromatic ring	Protein (tyrosine)
	Ring breathing modes	DNA (guanine, thymine)
745–765	Ethanolamine group	Phosphatidylethanolamine
	(δ) ring	Protein (tryptophan)
840–860	C—O—C skeletal mode in monosaccharides and disaccharide	α-Glucose and maltose
960–970	δ(═CH) wagging	Lipid
995–1015	Ring stretching modes of benzene derivatives	Protein (phenylalanine and tryptophan)
1075–1095	ν(C—C) or ν(C—O)	Lipid (phospholipids)
	O—P—O backbone stretching	DNA
1255–1265	Amide III (β-sheet and random coil)	Protein (secondary structure)
	Ring breathing modes	DNA (thymine and adenine)
1320–1330	Amide III (α-helix)	Protein (secondary structure)
	CH_3CH_2 wagging mode	DNA (guanine, adenine)
1455–1465	δ(CH_2) wagging,	Lipid
1600–1615	Amide I (antiparallel β-sheet)	Protein (secondary structure)
1660–1670	Amide I (α-helix)	Protein (secondary structure)

MM.1R and U266/BTZ-R Raman spectra show subtle differences compared to their sensitive equivalent, in terms of peaks positions and intensities, in the regions <1350 cm^{-1} (Fig. 4).

Both the resistant cells show modifications in the spectral region, ascribable to nucleic acids and proteins contributions (650–665, 740–775, 1075–1095, 1255–1265 and 1320–1330 cm^{-1}) compared to sentisitve cells. However, these signals differ in position and intensity, as evidenced in Fig. 4. Particularly, about MM.1S and MM.1R we observed a shift of peaks centered at 653, 757, 1082, 1259 and 1323 cm^{-1} to 661, 768, 1086, 1263 and 1330 cm^{-1}. Differently, about U266B1 and U266/BTZ-R we observed a shift of peaks centered at 657, 1090, 1263 and 1326 cm^{-1} to 661, 1086, 1259 and 1330 cm^{-1}. This behavior indicates different rearrangements of the protein and nucleic acids.

Exclusive difference between MM.1S and MM.1R spectra concerns a shift to lower wavenumber of peaks ascribable to C–O–C skeletal mode in mono- and disaccharide (from 847 to 843 cm^{-1}), ring stretching modes of benzene derivatives (from 1013 to 1010 cm^{-1}) and antiparallel β-sheet of Amide I in protein (from 1614 to 1607 cm^{-1}). On the other hand, exclusive difference between U266B1 and U266/BTZ-R spectra concerns a shift to lower wavenumber of peaks ascribable to ester group (from 549 to 545 cm^{-1}). Moreover a strong variation is observed in the region 745–765 cm^{-1}, ascribable to phosphatidylethanolamine and to tryptophan amino acid. More specifically, we observed the disappearance of peak at 749 cm^{-1} and the appearance of a new peak a 772 cm^{-1}.

To define the efficiency and sensitivity of the proposed approach for single-cell classification, we combined the Raman spectra analysis with a multivariate statistical method.

The results of the PCA analysis and of the subsequent HCA procedure are shown in Fig. 5, where the PC1 vs PC2 values are reported. The points enclosed in the two ellipses refer to the two clusters, as they were identified by the HCA algorithm. About MM.1 cell line, the two clusters contain 13 (cluster# 1) and 28 (cluster#2) spectra, respectively. More than the 62% of the variance is within the first two principal components (PC1 and PC2). Differently for U266B1, the two clusters contain 15 spectra for each subtype. The corresponding dendrograms, shown in Fig. 5C and D, are generated using the distance *cosine* criterion, the *correlation* one gives the same results.

4. Discussions

In this study we used MM cells that are considered to be useful model systems to explore mechanisms of resistance to DXM and BTZ. Raman spectra from sensitive and resistant cells appeared very similar but with subtle differences in intensities and positions of specific defined Raman peaks. The variations observed in the spectral regions of nucleic acids, lipids and proteins allow drug-sensitive and -resistant

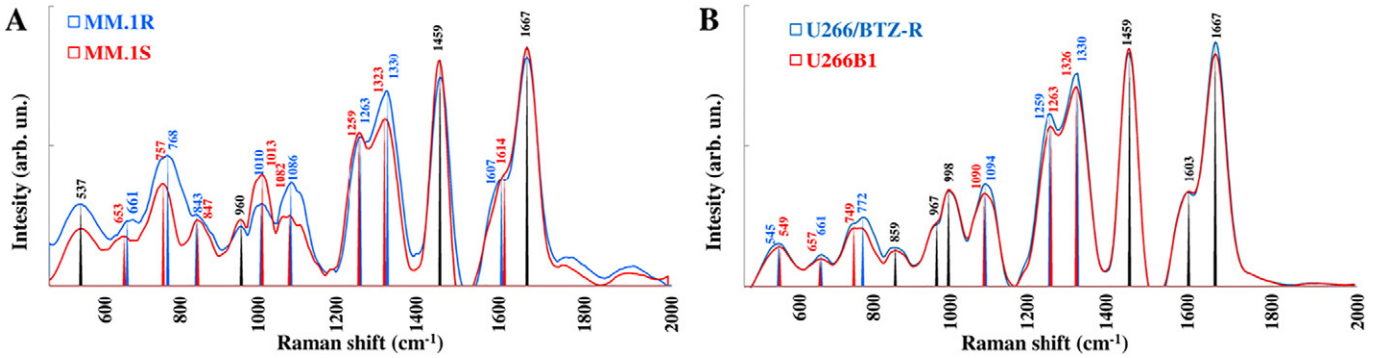

Fig. 4. Variability of main Raman peaks for MM.1S and MM.1R (A) and for U266B1 and U266/BTZ-R (B) cells. Blue and red peaks indicate the molecular fingerprint, identified for resistant and sensitive cell of MM.1 and U266B1.

cells distinction and a better understanding of the molecular variations between the cell lines subtypes.

Specifically, the phosphate backbone and nucleotides Raman contributions, observed in MM.1R, are shifted with respect to MM.1S, which could be due to a dynamic assessment of chromatin organization related to decondensation of chromatin structure. These features are usually associated to a high metabolic and transcriptional activity.

Similar consideration were reported by Pijanka, indicating as the Raman spectroscopy analysis of isolated nuclei allows the discrimination between two different subtypes cells of the same lineage [51]. These differences have also been considered the major determinant of vibrational spectra difference rather in proliferative status than tumorigenicity.

On the overall, the changes observed referred to variations in nuclear structural organization, similarly to what reported for other GC-resistant myeloma cell lines [52]. In this case, a strong correlation was found between the cell lines nuclear abnormality levels and the resistance index against GCs. Image cytometry evidenced the progressive chromatin condensation with large chromatin clumps heterogeneously distributed through the nucleus in the GC-resistant sub-lines of RPMI 8226. However, these changes were strikingly different from the variations observed in multidrug-resistant variant of human B

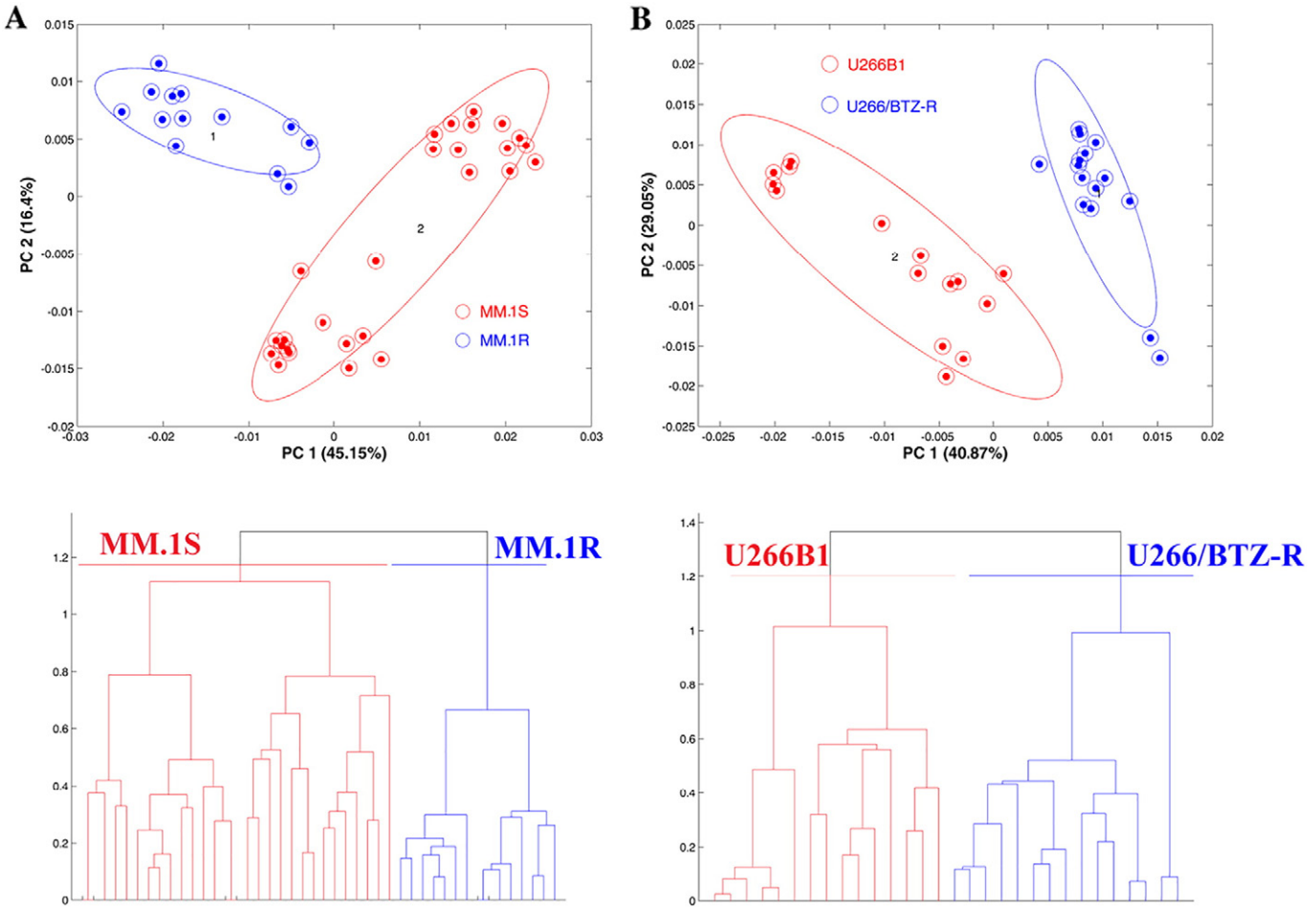

Fig. 5. PCA plot (PC2 vs PC1) obtained using the Raman spectra of MM.1S and MM.1R cells (A) and of U266B1 and U266/BTZ-R (B). Blue and red dots indicate cells identified by HCA analysis procedure as belonging to two distinct groups (C and D).

lymphoblastoid cell line, in which textural parameters indicates a chromatin decondensation with a less compact chromatin distribution and a finely granular and homogeneous aspect [52].

It is interesting to remark that, as we showed in a previous study [53] in 3% of analyzed cells, the acquisition of GC-resistance was associated with a reduced heat-stress resistance, which corresponded to a reduced mechanical strength of cell membrane. We connected this alteration to characteristic peaks corresponding to symmetric and asymmetric stretching bands of nucleic acids and lipids, suggesting a structural degradation of the corresponding cell macromolecules. It's known that GCs, such as DXM, are a class of corticosteroids commonly used in the treatment of MM and they are able to induce an effective response, even when used in monotherapy [54]. Their activity is carried out by the bond with GR that modulates important biologic processes, as cell proliferation and differentiation [55]. Resistance to GCs may be caused by an alteration of expression levels or amino acid sequence of GR, as a result of mutation [56,57].

On the other hand, proteasome inhibitors-resistance, such as resistance to BTZ, is often associated to a mutation and a genomic profile, resulting in overexpression of the Heat Shock Protein B8 (HSPB8) or in a cellular extrusion via the drug efflux transporter P-gp [58]. In fact, both MM.1R and U266/BTZ-R cell lines show shift of the peaks, ascribable to nucleic acid and protein with respect to the corresponding sensitive cell lines. In addition, U266/BTZ-R spectra show a shift of the peaks ascribed to cholesterol (from 549 to 545 cm^{-1}) and of phosphatidylethanolamine contribution in the 650–665 cm^{-1} region, suggesting that the drug-resistance could also concern an alteration of lipid membrane fluidity.

In mammalian cells, membrane fluidity is regulated by levels of cholesterol that interferes on transition to the solid gel state, and phosphatidylethanolamine, that increases rigidity of the lipid bilayer [59]. Changes in lipid composition are related to the malignancy of the tumor, including increased cell cycle progression, tumor growth and drug resistance [60].

Alteration of lipid membrane between testicular cancer cells sensible and resistant has just been reported in Movasaghi et al. In particular Raman CH region of nucleic acids, proteins and lipids, has just been used to discriminate resistant and sensitive cells [61].

Further Raman features in the regions of nucleic acid and proteins, defined in this work, indicate a significant rearrangement in the cell structural organization of both resistant cell lines. On the other hand, Raman signals appear to be specific for each resistant cell lines.

These findings can be used to discriminate sensitive and resistant cell by investigation of molecular pattern that lead to drug-resistant neoplastic cells.

By PCA analyses, sensitive and resistant subtype clusters resulted clearly separated, although a spreading of some clusters points out for the presence of subtle cell-to-cell variations within the same cell line. This evidence is due to a lack of cell synchronization and does not affect on the discrimination analysis by PCA.

5. Conclusions

On the basis of the previously discussed results, the proposed relatively simple empirical analysis allows to discriminate between sensitive and resistant cell subtypes in two myeloma multiple cell lines, using limited information contained in the original Raman spectra. Data treatment strongly limited both noise sources and spectral variability, allowing the discrimination of the sensitive and resistant cell samples with high sensitivity and specificity.

Moreover, by comparing Raman specific peaks, it has been possible to detect several cellular markers that can be used in the future to understand at the molecular level that lead to drug-resistant neoplastic cells.

To this purpose, the proposed method can be helpful in the speeding up of cell identification, even if further research is needed to verify whether analysis of patient cells could allow the identification of the resistance to a given drug or to a specific combination of drugs, in order to address the appropriate pharmacological choice, also ensuring therapeutic success.

Acknowledgements

Authors gratefully acknowledge A.B.A.L. onlus Messina (Italy) (http://www.abalmessina.it) for the use of the XploRA Raman spectrometer.

References

[1] A. Allegra, G. Penna, A. Alonci, S. Russo, B. Greve, V. Innao, V. Minardi, C. Musolino, Eur. J. Haematol. 90 (2013) 441–468.
[2] P.G. Richardson, B. Barlogie, J. Berenson J, S. Singhal, S. Jagannath, D. Irwin, S.V. Rajkumar, G. Srkalovic, M. Alsina, R. Alexanian, D. Siegel, R.Z. Orlowski, D. Kuter, S.A. Limentani SA, S. Lee, T. Hideshima, D.L. Esseltine, M. Kauffman, J. Adams, D.P. Schenkein, K.C. Anderson, N. Engl. J. Med. 348 (2003) 2609–2617.
[3] E. Kastritis, A. Palumbo, M.A. Dimopoulos, Semin. Hematol. 46 (2009) 143–157.
[4] W.S. Dalton, R. Jove, Semin. Oncol. 26 (1999) 23–27.
[5] M.V. Mateos, Cancer Treat. Rev. 36 (2010) S24–S32.
[6] P.G. Richardson, C. Mitsiades, T. Hideshima, K.C. Anderson, Cell Cycle 4 (2005) 290–296.
[7] A. Allegra, A. Alonci, D. Gerace, S. Russo, V. Innao, L. Calabrò, C. Musolino, Leuk. Res. 38 (2014) 1–9.
[8] I. Rogatsky, J.M. Trowbridge, M.J. Garabedian, Mol. Cell. Biol. 17 (1997) 3181–3193.
[9] S.H. Choi, S.W. Kim, D.H. Choi, B.H. Min, B.G. Chun, Leuk. Res. 24 (2000) 119–127.
[10] U. Nuutinen, S. Suoranta, J. Eeva, M. Eray, R. Pellinen, J. Wahlfors, J. Pelkonen, Leuk. Res. 33 (2009) 1714–1717.
[11] M.C. Marchetti, B.D. Marco, G. Cifone, G. Migliorati, C. Riccardi, Blood 101 (2003) 585–593.
[12] C.C. Chua, B.H.L. Chua, Z. Chen, L. Cathy, R.C. Hamdy, Biochim. Biophys. Acta 1642 (2003) 79–85.
[13] M.T. Abrams, N.M. Robertson, K. Yoon, E. Wickstrom, J. Biol. Chem. 279 (2004) 55809–55817.
[14] D. Chrysis, F. Zaman, A.S. Chagin, M. Takigawa, L. Sävendahl, Endocrinology 146 (2005) 1391–1397.
[15] S. Sharma, A. Lichtenstein, Blood 112 (2008) 1338–1345.
[16] S. Schmidt, J. Rainer, C. Ploner, E. Presul, S. Riml, R. Kofler, Cell Death Differ. 11 (2004) S45–S55.
[17] M.C. Marchetti, B.D. Marco, M.C. Santini, A. Bartoli, D.V. Delfino, C. Riccardi, Toxicol. Lett. 139 (2003) 175–180.
[18] P.S. Bachmann, R. Gorman, K.L. MacKenzie, L. Lutze-Mann, R.B. Lock, Blood 105 (2005) 2519–2526.
[19] Y. Gazitt, V. Fey, C. Thomas, R. Alvarez, Int. J. Oncol. 13 (1998) 397–405.
[20] A. Mahindra, J. Laubach, N. Raje, N. Munshi, P.G. Richardson, K. Anderson, Nat. Rev. Clin. Oncol. 9 (2012) 135–143.
[21] D.J. Kuhn, Z. Berkova, R.J. Jones, R. Woessner, C.C. Bjorklund, W. Ma, R.E. Davis, P. Lin, H. Wang, T.L. Madden, C. Wei, V. Baladandayuthapani, M. Wang, S.K. Thomas, J.J. Shah, D.M. Weber, R.Z. Orlowski, Blood 120 (2012) 3260–3270.
[22] A.J. Kale, B.S. Moore, J. Med. Chem. 55 (2012) 10317–10327.
[23] T. Liu, Z. Fei, K.J. Gangavarapu, S. Agbenowu, A. Bhushan, J.C.K. Lai, C.K. Daniels, S. Cao, Leuk. Res. 37 (2013) 1322–1328.
[24] J.J. Zhao, Z.B. Chu, Y. Hu, J. Lin, Z. Wang, M. Jiang, M. Chen, X. Wang, Y. Kang, Y. Zhou, T.N. Chonghaile, M.E. Johncilla, Y.T. Tai, J.Q. Cheng, A. Letai, N.C. Munshi, K.C. Anderson, R.D. Carrasco, Cancer Res. 75 (2015) 4384–4397.
[25] R. Oerlemans, N.E. Franke, Y.G. Assaraf, J. Cloos, I. van Zantwijk, C.R. Berkers, G.L. Scheffer, K. Debipersad, K. Vojtekova, C. Lemos, J.W. van der Heijden, B. Ylstra, G.J. Peters, G.L. Kaspers, B.A. Dijkmans, R.J. Scheper, G. Jansen, Blood 112 (2008) 2489–2499.
[26] J.J. Keats, R. Fonseca, M. Chesi, R. Schop, A. Baker, W.J. Chng, S. Van Wier, R. Tiedemann, C.X. Shi, M. Sebag, E. Braggio, T. Henry, Y.X. Zhu, H. Fogle, T. Price-Troska, G. Ahmann, C. Mancini, L.A. Brents, S. Kumar, P. Greipp, A. Dispenzieri, B. Bryant, G. Mulligan, L. Bruhn, M. Barrett, R. Valdez, J. Trent, A.K. Stewart, J. Carpten, P.L. Bergsagel, Cancer Cell 12 (2007) 131–144.
[27] D.H. Lee, K. Chung, J.A. Song, T.H. Kim, H. Kang, J.H. Huh, S.G. Jung, J.J. Ko, H.J. An, J. Proteome Res. 9 (2010) 5668–5676.
[28] M. Gutova, J. Najbauer, A. Gevorgyan, M.Z. Metz, Y. Weng, C.-C. Shih, K.S. Aboody, PLoS One 28 (2007), e243. .
[29] V. Genty, G. Dine, J. Dufer, Leuk. Res. 28 (2004) 307–313.
[30] I.S. Song, H.K. Kim, S.R. Lee, S.H. Jeong, N. Kim, K.S. Ko, B.D. Rhee, J. Han, Int. J. Cancer 133 (2013) 1357–1367.
[31] J. Chan, S. Fore, S. Wachsmann-Hogiu, T. Huser, Laser Photonics Rev. 2 (2008) 325–349.
[32] I.W. Schie, L. Alber, A.L. Gryshuk, J.W. Chan, Analyst 139 (2014) 2726–2733.
[33] N. Stone, P. Matousek, Cancer Res. 68 (2008) 4424–4430.
[34] P.R. Carey, J. Biol. Chem. 274 (1999) 26625–26628.
[35] S. Greenstein, N.L. Krett, Y. Kurosawa, C. Ma, D. Chauhan, T. Hideshima, K.C. Anderson, S.T. Rosen, Exp. Hematol. 31 (2003) 271–282.
[36] J. Park, E.-K. Bae, C. Lee, J.-H. Choi, W.J. Jung, K.-S. Ahn, S.-S. Yoon, BMB Rep. 47 (2014) 274–279.

[37] M. Schoester, M. Van Duin, Y. De Knegt, S.L. Corthals, A. Broyl, P. Sonneveld, Haematologica 93 (s1) (2008) 314, Abs.0786. .
[38] Z.M. Zhang, S. Chen, Y.Z. Liang, Analyst 135 (2010) 1138–1146.
[39] A. Savitzky, M.J.E. Golay, Anal. Chem. 36 (1964) 1627–1639.
[40] I.S. Patel, W.R. Premasiri, D.T. Moir, L.D. Ziegler, J. Raman Spectrosc. 39 (2008) 1660–1672.
[41] R. Gautam, S. Vanga, F. Ariese, S. Umapathy, EPJ Techniques and Instrumentation 2 (2015) 1–38 (AAAAAA).
[42] J.W. Chan, D.S. Taylor, T. Zwerdling, S.M. Lane, K. Ihara, T. Huser, Biophys. J. 90 (2006) 648–656.
[43] E. Fazio, S. Trusso, D. Franco, M.S. Nicolò, A. Allegra, F. Neri, C. Musolino, S.P.P. Guglielmino, Spectrochim. Acta A Mol. Biomol. 159 (2016) 21–29.
[44] C. Krafft, L. Neudert, T. Simat, R. Salzer, Spectrochim. Acta A Mol. Biomol. 61 (2005) 1529–1535.
[45] W.T. Cheng, M.T. Liu, H.N. Liu, S.Y. Lin, Microsc. Res. Tech. 68 (2005) 75–79.
[46] G. Shetty, C. Kedall, N. Shepherd, N. Stone, H. Barr, Brit. J. Cancer 94 (2006) 1460–1464.
[47] R.E. Kast, G.K. Serhatkulu, A. Cao, A.K. Pandya, H. Dai, J.S. Thakur, V.M. Naik, R. Naik, M.D. Klein, G.W. Auner, R. Rabah, Biopolymers 89 (2008) 235–241.
[48] P. Cipriani, C.Y. Smith, Spectrochem. Acta. A Mol. Biomol. 69 (2008) 333–337.
[49] Z. Huang, A. McWilliams, M. Lui, D.I. McLean, S. Lam, H. Zeng, Int. J. Cancer 107 (2003) 1047–1052.
[50] R.J. Lakshimi, V.B. Kartha, C.M. Krishna, J.G.R. Solomon, G. Ullas, P. Uma Devi, Radiat. Res. 157 (2002) 175–182.
[51] J.K. Pijanka, N. Stone, A.V. Rutter, N. Forsyth, G.D. Sockalingum, Y. Yang, J. Sulé-Suso, Analyst 138 (2013) 5052–5058.
[52] V. Genty, V. El-Khoury, F. Liautaud-Roger, G. Dine, J. Dufer, Cancer Biol. Ther. 4 (2005) 832–839.
[53] A. Allegra, E. Fazio, D. Franco, M. Nicolò, S. Trusso, F. Neri, C. Musolino, S. Guglielmino, Leuk. Lymphoma 56 (2015) 1514–1516.
[54] S. Kumar, M.Q. Lacy, A. Dispenzieri, S.V. Rajkumar, R. Fonseca, S. Geyer, C. Allmer, T.E. Witzig, J.A. Lust, P.R. Greipp, R.A. Kyle, M.R. Litzow, M.A. Gertz, Bone Marrow Transplant. 34 (2004) 485–490.
[55] D.J. Mangelsdorf, C. Thummel, M. Beato, P. Herrlich, G. Schütz, K. Umesono, B. Blumberg, P. Kastner, M. Mark, P. Chambon, R.M. Evans, Cell 83 (1995) 835–839.
[56] P.A. Moalli, S. Pillay, D. Weiner, R. Leikin, S.T. Rosen, Blood 79 (1992) 213–222.
[57] B. Sánchez-Vega, V. Gandhi, Br. J. Haematol. 144 (2009) 856–864.
[58] D. Gutman, A.A. Morales, L.H. Boise, Leukemia 23 (2009) 2181–2183.
[59] R. Dawaliby, C. Trubbia, C. Delporte, C. Noyon, J.-M. Ruysschaert, P. Van Antwerpen, C. Govaerts, J. Biol. Chem. 291 (2016) 3658–3667.
[60] V. Lladó, D.J. López, M. Ibarguren, M. Alonso, J.B. Soriano, P.V. Escribá, X. Busquets, Biochim. Biophys. Acta 1838 (2014) 1619–1627;
C. Huang, C. Freter, Int. J. Mol. Sci. 16 (2015) 924–949.
[61] Z. Movasaghi, S. Rehman, I. ur Rehman, Appl. Spectrosc. Rev. 47 (2012) 571–581.